Published in final edited form as:

Science. 2019 October 18; 366(6463): 364–369. doi:10.1126/science.aay2204.

Light-driven deracemization enabled by excited-state electron transfer

Nick Y. Shin[1], **Jonathan M. Ryss**[2], **Xin Zhang**[1], **Scott J. Miller**[2,*], **Robert R. Knowles**[1,*]

[1]Department of Chemistry, Princeton University, Princeton NJ 08544 (USA).

[2]Department of Chemistry, Yale University, New Haven CT 06520 (USA).

Abstract

Deracemization is an attractive strategy for asymmetric synthesis, but intrinsic energetic challenges have limited its development. Here we report a deracemization method whereby amine derivatives undergo spontaneous optical enrichment upon exposure to visible light in the presence of three distinct molecular catalysts. Initiated by an excited-state iridium chromophore, this reaction proceeds *via* a sequence of favorable electron, proton, and hydrogen atom transfer steps that serve to break and reform a stereogenic C–H bond. The enantioselectivity in these reactions is jointly determined by two independent stereoselective steps that occur in sequence within the catalytic cycle, giving rise to a composite selectivity that is higher than that of either step individually. These reactions represent a distinct approach to creating out-of-equilibrium product distributions between substrate enantiomers using excited-state redox events.

One Sentence Summary:

Racemic amine derivatives undergo spontaneous optical enrichment upon exposure to visible light in the presence of three distinct small-molecule catalysts.

Enantioselective reactions are essential to the pharmaceutical, agrochemical, and fine chemical industries, providing access to products enriched in just one of two mirror-image geometries. Conventional enantioselective methods either transform achiral starting materials into chiral products or rely on kinetic resolutions to differentially transform the stereoisomers of chiral reactants. Both approaches have been the subject of extensive interest and development (1). In contrast, methods for achieving selective deracemization—wherein a racemic mixture of a given compound is wholly transformed into a single enantiomer of

---

*Correspondence to: rknowles@princeton.edu & scott.miller@yale.edu.

Author contributions: All authors contributed to the conceptualization of the project, the planning of experiments, and interpretation of results. R.R.K and S.J.M directed the research. N.Y.S., J.M.R., and X.Z. conducted the experiments. N.Y.S. and R.R.K. wrote the manuscript with input from all the authors.

Competing interests: The authors declare no competing financial interest.

Data and materials availability: Data are supplied in supplementary materials

Supplementary Materials:
Materials and Methods
Figures S1–S5
Tables S1–S8
References (30–46)

the same molecule—are rare, despite their conceptual simplicity and potential practical benefits (Fig. 1A) (2–4). Two factors complicate the development of deracemization methods. First, the conversion of a racemic mixture into a single enantiomer is unfavorable on thermodynamic grounds due to an attendant decrease in entropy. Although this effect is small (ΔG^{o} = +0.42 kcal/mol at 298 K), it requires that an additional source of energy be supplied to drive the reaction forward. The second challenge is kinetic in nature, and relates to the principle of microscopic reversibility (5). As enantiomers are equal in energy by definition, any series of elementary steps along a single potential surface that converts (*S*) to (*R*) will be equally facile in the reverse direction that transforms (*R*) to (*S*). In the absence of an exogenous driving force, this necessarily results in an equilibrium (racemic) distribution of products. Accordingly, effective deracemizations require both an input of energy to impart reaction directionality and distinct mechanisms for the elementary steps which respectively create and destroy stereochemistry.

Seminal examples from Turner, Toste, Zhou, and others have demonstrated that these requirements can be met through sequential redox transformations fueled by chemically compatible (or phase separated) oxidants and reductants, wherein the oxidation and reduction reactions occur independently and in parallel (6–8). Though effective, this approach can be challenging to generalize and requires that two stoichiometric reagents be consumed each time a molecule of substrate is processed. Excited-state reactions can also satisfy these key mechanistic requirements. As they occur across two distinct potential energy surfaces, photochemical transformations are not subject to detailed balance and can provide access to non-Boltzmann product distributions—a benefit that underlies the success of many classical photoisomerization reactions (9, 10). Moreover, from a practical perspective such processes require no chemical reagents, produce no stoichiometric waste, and consume nothing but photons. Along these lines, Bach and co-workers very recently reported ground-breaking examples of photo-driven deracemizations of allenes and cyclopropylquinolones utilizing a chiral photosensitizer that exhibits different energy-transfer efficiencies for the two substrate enantiomers, resulting in high levels of optical enrichment (Fig. 1C) (11, 12). These and other photoisomerizations are generally understood to proceed *via* the electronic excited states of the substrates themselves, which strategically defines a substrate-specific paradigm (13–15).

We present here a complementary platform for light-driven deracemizations based on the use of excited-state redox events (Fig. 1B). These electron transfer-based approaches provide an alternative mechanism for driving reactions in opposition to a thermodynamic gradient, yet are likely applicable to a wider range of substrates and reaction types than direct excitation or energy transfer-based approaches. We have previously shown that excited-state redox events can be used to drive out-of-equilibrium reactions, such as intermolecular olefin hydroaminations and the isomerization of cyclic alcohols to linear ketones, wherein the reaction products are higher in energy than the starting materials (16, 17). Here, we extend these studies and describe a method for the light-driven deracemization of cyclic ureas mediated by a ternary catalyst system comprising an Ir(III)-based photoredox catalyst, a BINOL-derived chiral phosphate base, and a cysteine-containing peptide thiol H-atom donor (Fig. 1D). This process occurs through a series of favorable electron transfer, proton transfer, and hydrogen atom transfer events that serve to break and reform a

stereogenic methine C–H bond. The extent of optical enrichment in these reactions is jointly determined by two independent enantioselective steps that proceed in sequence within the catalytic cycle. This results in an unusual (and beneficial) outcome in which two modestly stereoselective steps together result in an observed selectivity that is higher than that of either individual step. The discovery, optimization, scope, and a preliminary mechanistic model for this process are presented herein.

We first observed deracemization behavior serendipitously while attempting to develop an asymmetric variant of a previously reported hydroamidation reaction mediated by an Ir(III)-based photoredox catalyst, a dialkyl phosphate base, and an aryl thiol H-atom donor under visible light irradiation (Fig. 2A) (18). We found that the use of chiral BINOL phosphates as Brønsted bases was effective in this chemistry, and resulted in a modest level of enantioselectivity. However, time-course studies surprisingly revealed that the urea product **1b** was initially formed as a racemate but became slightly optically enriched during the course of the reaction. In subsequent control reactions, we subjected racemic **1b** to the reaction conditions and observed significant optical enrichment with near complete material recovery, indicating that a light-driven deracemization pathway was operative. Similarly, when enantiopure *(S)*-**1b** was subjected to identical conditions using an achiral phosphate base, racemization of the stereogenic C–H bond was observed.

Based on this discovery we postulated that the excited state of the Ir photocatalyst reversibly oxidizes the racemic urea substrate to form a mixture of transient (and enantiomeric) arene radical cations (Fig 2B). The stereogenic C–H bond in the resulting substrate radical cation is markedly acidified and can be deprotonated by the phosphate base to form a neutral a-amino radical (19, 20). However, as both the radical cation and the Brønsted base are chiral, this process serves to kinetically resolve the enantiomeric radical cations, with the fast-reacting (*R*)-enantiomer undergoing proton transfer while the slower-reacting (*S*)-enantiomer is converted back to urea starting material *via* charge recombination with the reduced Ir(II) state of the photocatalyst. In this way the reaction becomes enriched in the slower reacting (*S*)-enantiomer. Following proton transfer, the resulting a-amino radical intermediate can be reduced *via* H-atom transfer with the achiral aryl thiol co-catalyst to return the closed-shell urea in a non-selective process. A protoncoupled electron transfer (PCET) event between the reduced Ir(II) complex, thiyl, and protonated base could then return the active forms of all three catalysts.

If operational, this mechanism suggests that the two steps that create and destroy stereochemistry in these reactions—proton transfer and hydrogen-atom transfer—operate independently of one another and are mediated by two independent catalysts. Accordingly, when both the proton- and H-atom transfer catalysts are chiral, both elementary steps can potentially be rendered enantioselective, resulting in an unusual circumstance in which the observed stereoselectivity should be the product of the enantiomeric ratios for each of the two enantioselective steps ($er_{obs} = er_{PT} \bullet er_{HAT}$).

To evaluate this hypothesis, we elected to further study the deracemization of *N*-aryl substituted cyclic ureas. Preliminary studies demonstrated that a pendant amide hydrogen-bond donor group is crucial for obtaining high selectivities in the enantioselective

deprotonation step using the chiral phosphate bases (*vide infra*), prompting us to evaluate the deracemization of urea **2a** as a model substrate (Fig. 3A). A small collection of BINOL-derived phosphate bases were explored with $[Ir(dF(CF_3)ppy)_2(bpy)]PF_6$ (**Ir**) and an achiral thiophenol H-atom donor catalyst in tetrahydrofuran under irradiation with blue LEDs at room temperature. While a BINOL-derived phosphate with 1-adamantyl groups **(3a**) gave essentially racemic product, an analogous catalyst bearing phenyl groups gave an improved er of 69:31 (**3b**) (entries 1–2). We hypothesized that there might be a stabilizing π-cation interaction between oxidized substrate radical cation and the aryl substituents of chiral phosphate, prompting us to examine catalysts bearing more expansive aryl substituents (21). This in turn led to catalyst **3e** which gave 79:21 er and good yield (entries 3–5). The addition of molecular sieves further improved the selectivity to 86:14 er (entry 6).

We then investigated cysteine-based oligopeptides as enantioselective H-atom transfer catalysts. Although cysteine residues are known to mediate H-atom transfer reactions in a variety of biological contexts, they have only occasionally been explored for use in small-molecule asymmetric catalysis, and their study for catalytic asymmetric H-atom transfer is not yet reported (22–25). A small library of tetrapeptide disulfides (which are in equilibrium with their free thiol form under the reaction conditions) were initially screened with a catalytic amount of achiral tetrabutylammonium diphenylphosphate base, providing a lead result of 68:32 er with peptide **4b** (entries 7–9). The corresponding thiol **4c** gave a slightly improved er of 70:30 (entry 10). Variations at *i*+2 and *i*+3 positions demonstrated that cysteine-embedded tetrapeptide with phenylglycine as the C-terminal residue show improved er, leading to **4e** with 78:22 er and good yield (entries 11–12). The use of molecular sieves slightly improved the selectivity to 79:21 er (entry 13). With optimized chiral phosphate **3e** and chiral thiol **4e** in hand, our mechanistic hypothesis predicted that reactions mediated by the stereochemically matched pair of catalysts should result in an observed er of 96:4 (86:14 • 79:21 = 96:4) (26). Gratifyingly, reaction of *rac*- **2a** with **3e**, **4e**, Ir, and molecular sieves indeed produced optically enriched **2a**, with a composite selectivity of 93:7 er (entry 14) upon irradiation with blue LEDs. We speculated that the modest deviation from the predicted er value might result from a thiyl-mediated racemization pathway that may become operative at high levels of optical enrichment (27). We postulated that inclusion of an alternative H-atom donor with a much weaker C–H bond might react preferentially with the alkyl thiyl radical and suppress any undesired racemization. Accordingly, we were pleased to find that addition of 50 mol% triphenylmethane to the optimal conditions improved the er to the expected value of 96:4 (entry 15). Further investigation revealed that use of lower catalyst loadings was also effective (entry 16). Control reactions revealed that exclusion of light or any of the reaction components resulted in either complete loss of optical enrichment or diminished levels of enantioselectivity (Table S1).

With these optimized deracemization conditions in hand, we found that a variety of structural changes in the urea substrate could be accommodated (Fig. 3B). Alkyl substituents of varying steric demand could be tolerated at the stereogenic carbon with uniformly good levels of enantioselectivity (**2a**–**2e**). Substitution of the distal urea nitrogen with the free N–H amide, benzyl, or isopropyl groups also provided the desired deracemized products with

high levels of stereoselectivity (**2f**–**2h**). Structural changes on the acyclic amide moiety were also tolerated, as was a benzamide derivative (**2i**–**2n**). However, a N,N-dimethyl amide variant demonstrated a noticeable decrease in the er (**2o**). Upon reaching the steady-state level of optical enrichment, all the substrates studied here **2a**–**2o** can be recovered in nearly quantitative yield.

Numerous observations are consistent with the mechanistic proposal outlined above (Fig. 4A). Steady-state Stern–Volmer quenching studies and time-correlated single photon counting experiments revealed that electron transfer between the urea substrate ($E_{p/2}$ = 0.91 V vs. Fc^+/Fc in MeCN, Fig. S1) and the excited-state of **Ir** (*$E_{1/2}$ = 0.94 V vs. Fc^+/Fc in MeCN) (28) is kinetically rapid (k_{ET} for (*R*)-***2a*** and (*S*)-***2a*** = 9.0(8)×10^8 $M^{-1}s^{-1}$ and 8.8(7) ×10^8 $M^{-1}s^{-1}$, Fig. S2). The subsequent proton transfer, H-atom transfer, and PCET steps are also thermodynamically favorable (Fig. S3). These findings reinforce the notion that, as all the elementary steps proceeding from ***Ir** are exergonic, the observed product distributions are kinetically controlled and fully decoupled from the energetic difference between the racemic starting material and optically enriched product. The steady-state er is achieved within only 1.5 hours, and no degradation of either yield or er was observed upon extended reaction times, suggesting that the system establishes a stable non-equilibrium state (Fig. 4B). The quantum yield of this process was measured to be 4.8(3)% (Fig. S5) (29). Lastly, we found that catalyst-controlled stereoinversion from optically pure *(S)*-**2a** to *(R)*-**2a** could be achieved under the optimized condition with excellent er and reaction efficiency (Fig. 4C).

To investigate the generality of proposed synergistic stereoselectivity between the two chiral catalysts, the enantioselectivity of each catalyst was explored individually for a selected set of substrates (Table 1). First, substrates were subjected to deracemization with chiral base **3e** and thiophenol as an achiral H-atom transfer catalyst – conditions that will directly report on the er of the proton transfer step. The observed er was generally consistent for substrates bearing a pendant amide group (entries 1–10). Methylation of the amide N–H or removal of the pendant amide group significantly decreased the er (entry 11–12), which supports a potential interaction between the distal amide N–H bond and phosphate base during the asymmetric proton transfer step. The same substrates were then deracemized with cysteine-embedded peptide **4e** and tetrabutylammonium diphenylphosphate as an achiral Brønsted base catalyst, providing a measure of the selectivity in the H-atom transfer step. Though substitution of the urea backbone led to small variations, the enantioselectivity in the HAT step is similar for all substrates with or without the pendant amide group. Gratifyingly, when the stereochemically matched forms of both chiral catalysts were employed (e.g the phosphate selectively ablates the *(S)* enantiomer while the thiol preferentially reforms the (*R*) enantiomer), the resultant er value closely matched the predicted value in all cases. Similarly, the combination of mismatched thiol *ent*-**4e** with base **3e** provided significantly diminished er for **2a**, indicating conflicting stereochemical preferences wherein the deprotonation and HAT events both favor the (*S*) enantiomer (entry 2). These observations are consistent with the proposed mechanism and highlight the synergistic role of the two chiral catalysts in this transformation.

We anticipate that the mechanistic features underlying this work are general, and may be adapted to a wide variety of other light-driven transformations to provide non-equilibrium product distributions in a catalyst-controlled fashion.

Supplementary Material

Refer to Web version on PubMed Central for supplementary material.

Acknowledgements

We thank Casey B. Roos, Hunter H. Ripberger, and Dr. Brendan C. Lainhart for preliminary studies and the synthesis of catalysts. We also acknowledge Dr. Anthony J. Metrano, Dr. Christopher R. Shugrue, and Aaron L. Featherston for helpful discussions, as well as Zi S. D. Toa and Qilei Zhu for technical assistance. R.R.K thanks David MacMillan for many stimulating discussions about deracemization over the past 12 years.

Funding: Support for this work was provided by NIH R01 GM120530 (R.R.K.) and NIH R35 GM132092 (S.J.M.). J.M.R. acknowledges the Department of Defense (DoD) for funding through the National Defense Science & Engineering Graduate Fellowship (NDSEG) Program.

References and Notes

1. Comprehensive Asymmetric Catalysis. Vol. I —III Edited by Jacobsen EN, Pfaltz A, and Yamamoto H. Springer-Verlag, Berlin (1999).
2. Carnell AJ, Biotransformations, 57–72 (2001).
3. Servi S, Tessaro D, Pedrocchi-Fantoni G. Coord. Chem Rev 252, 715–726 (2008).
4. Kroutil W, Faber K, Tetrahedron: Asymmetry, 9, 2901–2913 (1998).
5. Blackmond DG. Angewandte Chemie Int Ed. 48, 2648–2654 (2009).
6. Lackner AD, Samant AV, Toste DF. J. Am. Chem. Soc 135, 14090–14093 (2013). [PubMed: 24025122]
7. Alexeeva M, Enright A, Dawson M, Mahmoudian M, Turner N, Angew. Chem. Int. Ed, 41, 3177–3180 (2002).
8. Ji Y, Shi L, Chen M-W, Feng G-S, Zhou Y-G. J. Am. Chem. Soc 137, 10496–10499 (2015). [PubMed: 26274896]
9. Kathan M, Hecht S. Chem. Soc. Rev 46, 5536–5550 (2017). [PubMed: 28857096]
10. Astumian R, Faraday Discuss. 195, 583–597 (2016). [PubMed: 27768148]
11. Hölzl-Hobmeier A et al., Nature. 564, 240–243 (2018). [PubMed: 30542163]
12. Tröster A, Bauer A, Jandl C, T. *Angew. Chem. Int. Ed*. 58, 3538–3541 (2019).
13. Metternich JB, Gilmour R, J. Am. Chem. Soc, 137, 11254–11257 (2015). [PubMed: 26310905]
14. Singh K, Staig SJ, Weaver JD. J. Am. Chem. Soc 136, 5275–5278 (2014). [PubMed: 24678625]
15. Metternich JB, Gilmour R, J. Am. Chem. Soc, 138, 1040–1045 (2016). [PubMed: 26714650]
16. Ota E, Wang H, Frye N, Knowles RR. J. Am. Chem. Soc 141, 1457–1462 (2019). [PubMed: 30628777]
17. Musacchio AJ et al. Science. 355, 727–730 (2017). [PubMed: 28209894]
18. Miller DC, Choi GJ, Orbe HS, Knowles RR. J. Am. Chem. Soc 137, 13492–5 (2015). [PubMed: 26439818]
19. Beatty JW, Stephenson CR. Acc. Chem. Res 48, 1474–84 (2015). [PubMed: 25951291]
20. McNally A, Prier CK, MacMillan DW, Science. 334, 1114–1117 (2011). [PubMed: 22116882]
21. Kennedy RC, Lin S, Jacobsen EN, Angew. Chem. Int. Ed 55, 12596–12624 (2016).
22. Ryss JM, Turek AK, Miller SJ, Org. Lett 20, 1621–1625 (2018). [PubMed: 29504763]
23. Aroyan CE, Miller SJ. J. Am. Chem. Soc 129, 256–257 (2007). [PubMed: 17212388]
24. Hashimoto T, Kawamata Y, K. Maruoka. Nat. Chem 6, 702–705 (2014).
25. Haque MB, Roberts BP, Tocher DA. J. Chem Soc. Perkin Trans. 1 2881–2889 (1998)

26. Masamune S, Choy W, Petersen JS, Sita LR. Angew. Chem. Int. Ed 24, 1–30 (1985).
27. Loh Y et al., Science. 358, 1182–1187 (2017). [PubMed: 29123019]
28. Hanss D, Freys JC, Bernardinelli G, Wenger OS, Eur. J. Inorg. Chem 32, 4850–4859 (2009).
29. Hatchard CG, Parker CA, Proceedings of the Royal Society of London. Series A, Mathematical and Physical Sciences, 235, 518–536 (1956).

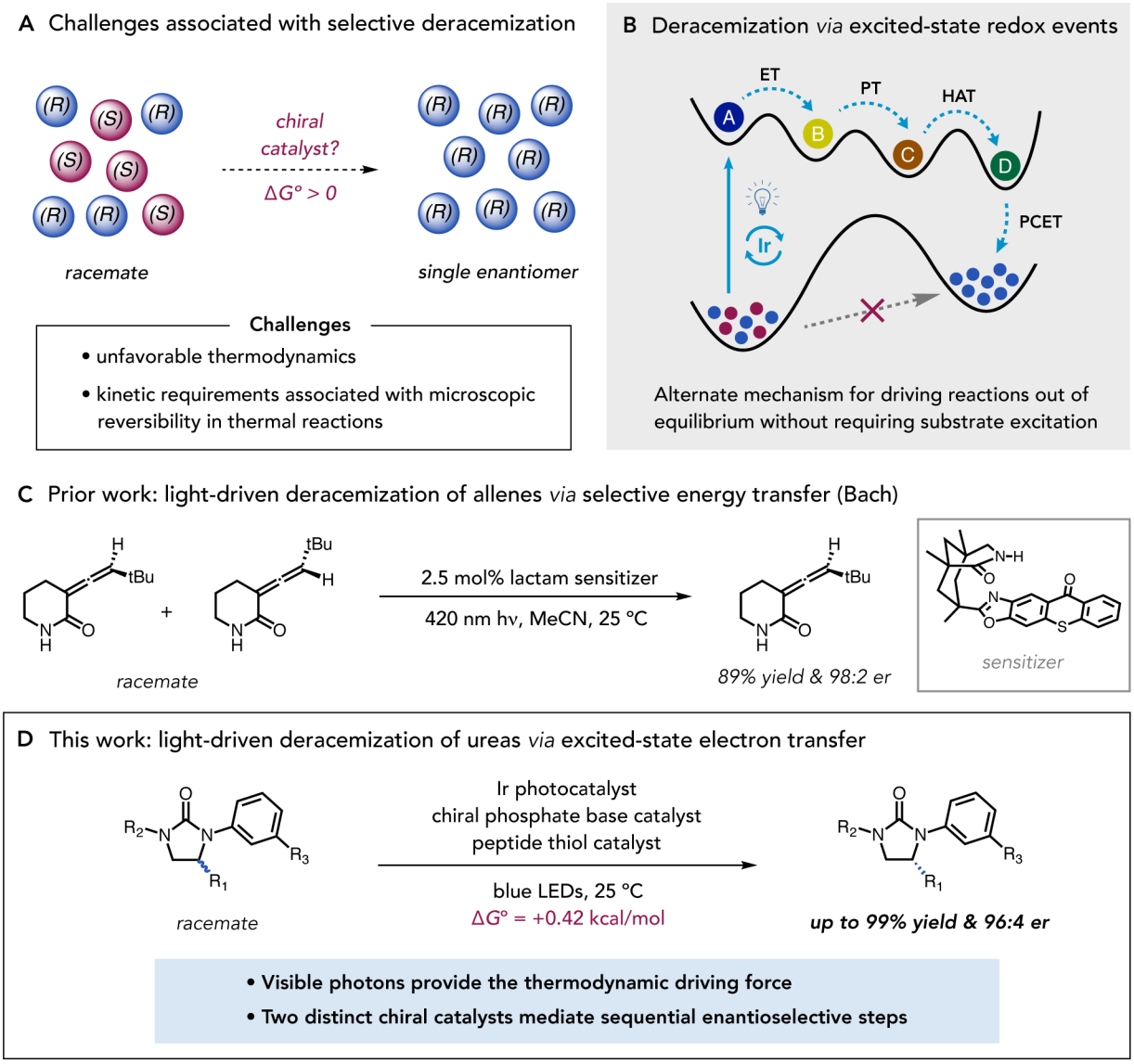

Fig. 1. Reaction development.

(A) Thermodynamic and kinetic challenges in developing methods for selective deracemization. (B) General, light-driven strategies for achieving out-of-equilibrium deracemization through excited-state redox events. (C) Bach's report on light-driven deracemization *via* selective energy transfer. (D) Light-driven deracemization of cyclic ureas by excited-state electron transfer.

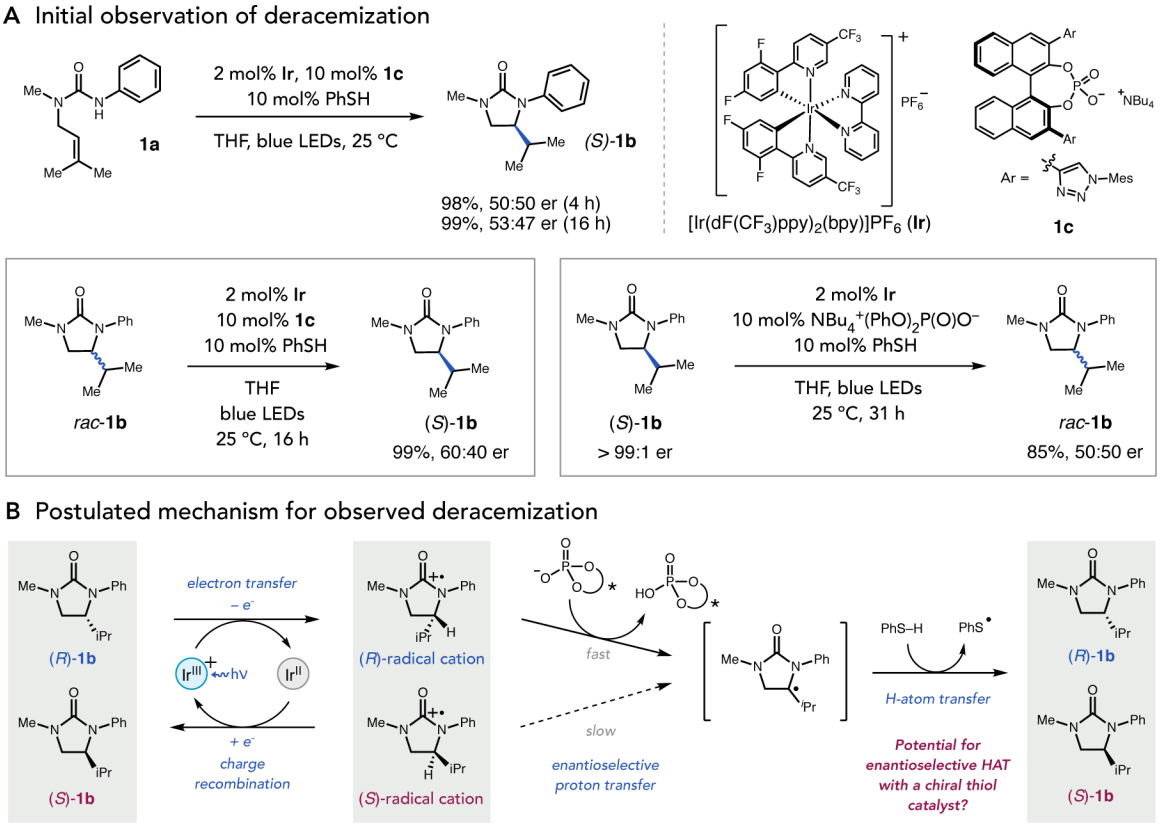

Fig. 2. Discovery of light-driven deracemization

(A) Initial observations. Ir is racemic in all experiments. (B) Postulated mechanism.

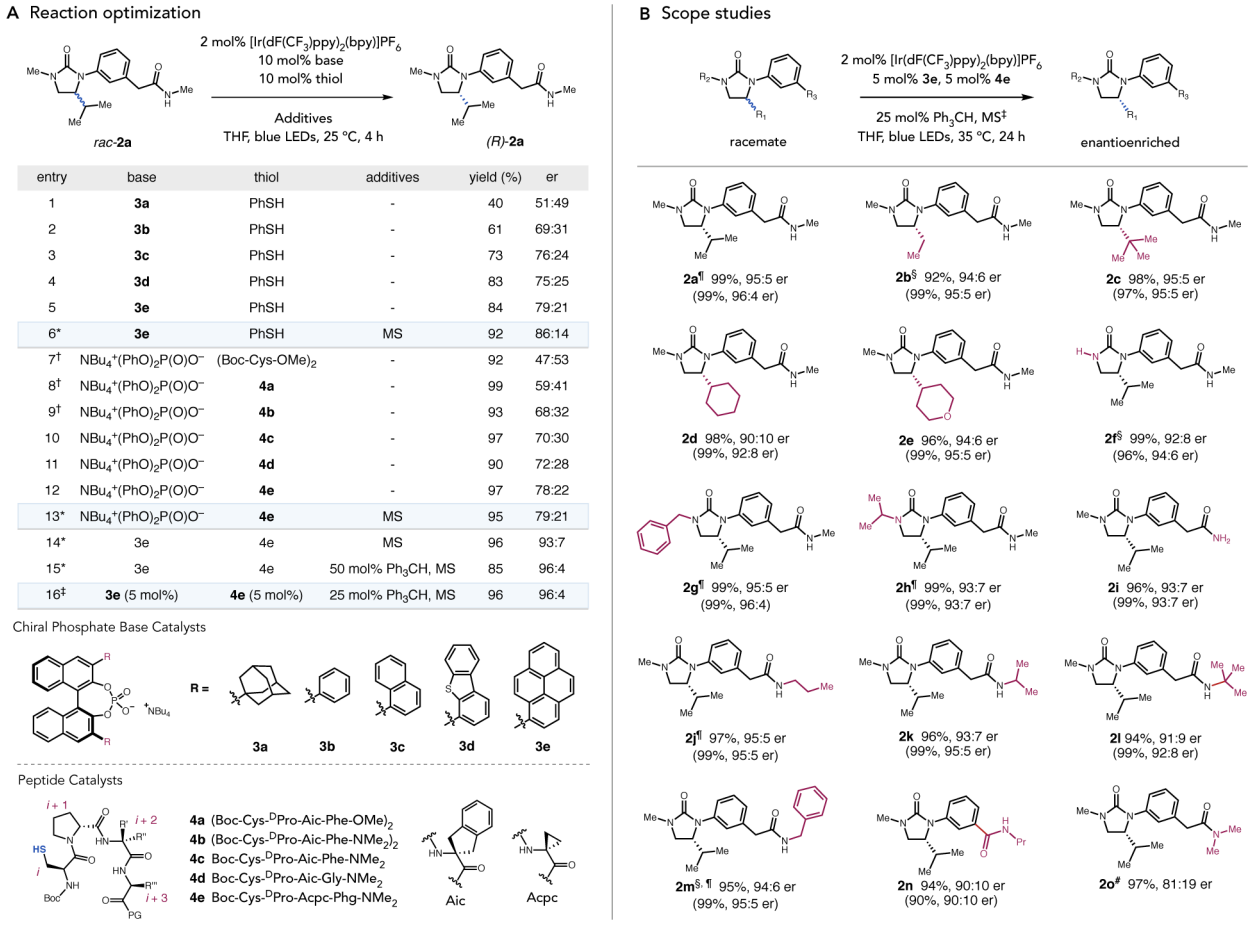

entry	base	thiol	additives	yield (%)	er
1	**3a**	PhSH	-	40	51:49
2	**3b**	PhSH	-	61	69:31
3	**3c**	PhSH	-	73	76:24
4	**3d**	PhSH	-	83	75:25
5	**3e**	PhSH	-	84	79:21
6*	**3e**	PhSH	MS	92	86:14
7†	$NBu_4^+(PhO)_2P(O)O^-$	$(Boc\text{-}Cys\text{-}OMe)_2$	-	92	47:53
8†	$NBu_4^+(PhO)_2P(O)O^-$	**4a**	-	99	59:41
9†	$NBu_4^+(PhO)_2P(O)O^-$	**4b**	-	93	68:32
10	$NBu_4^+(PhO)_2P(O)O^-$	**4c**	-	97	70:30
11	$NBu_4^+(PhO)_2P(O)O^-$	**4d**	-	90	72:28
12	$NBu_4^+(PhO)_2P(O)O^-$	**4e**	-	97	78:22
13*	$NBu_4^+(PhO)_2P(O)O^-$	**4e**	MS	95	79:21
14*	3e	4e	MS	96	93:7
15*	3e	4e	50 mol% Ph_3CH, MS	85	96:4
16‡	**3e** (5 mol%)	**4e** (5 mol%)	25 mol% Ph_3CH, MS	96	96:4

Fig. 3. Reaction optimization and scope studies.

(A) Optimization of reaction conditions. Reactions were performed on 0.025 mmol scale. Yields were determined by ^{1}H NMR analysis of crude reaction mixtures relative to an internal standard. The er was determined by HPLC analysis on a chiral stationary phase. *10 %m/v of molecular sieves (MS) †5 mol% of disulfide ‡5 %m/v of MS. (B) Reaction scope. Reactions were run at 0.25 mmol scale unless otherwise noted. Yields and er values are for isolated material after purification and are the average of two experiments. In parentheses are yields and er's obtained on 0.025 mmol scale analyzed by ^{1}H NMR and HPLC analysis, in which the internal reaction temperature was measured to be 25 °C. §Reaction scale = 0.10 mmol. ¶Reaction time = 12 h. #Reaction scale = 0.025 mmol, NMR yield.

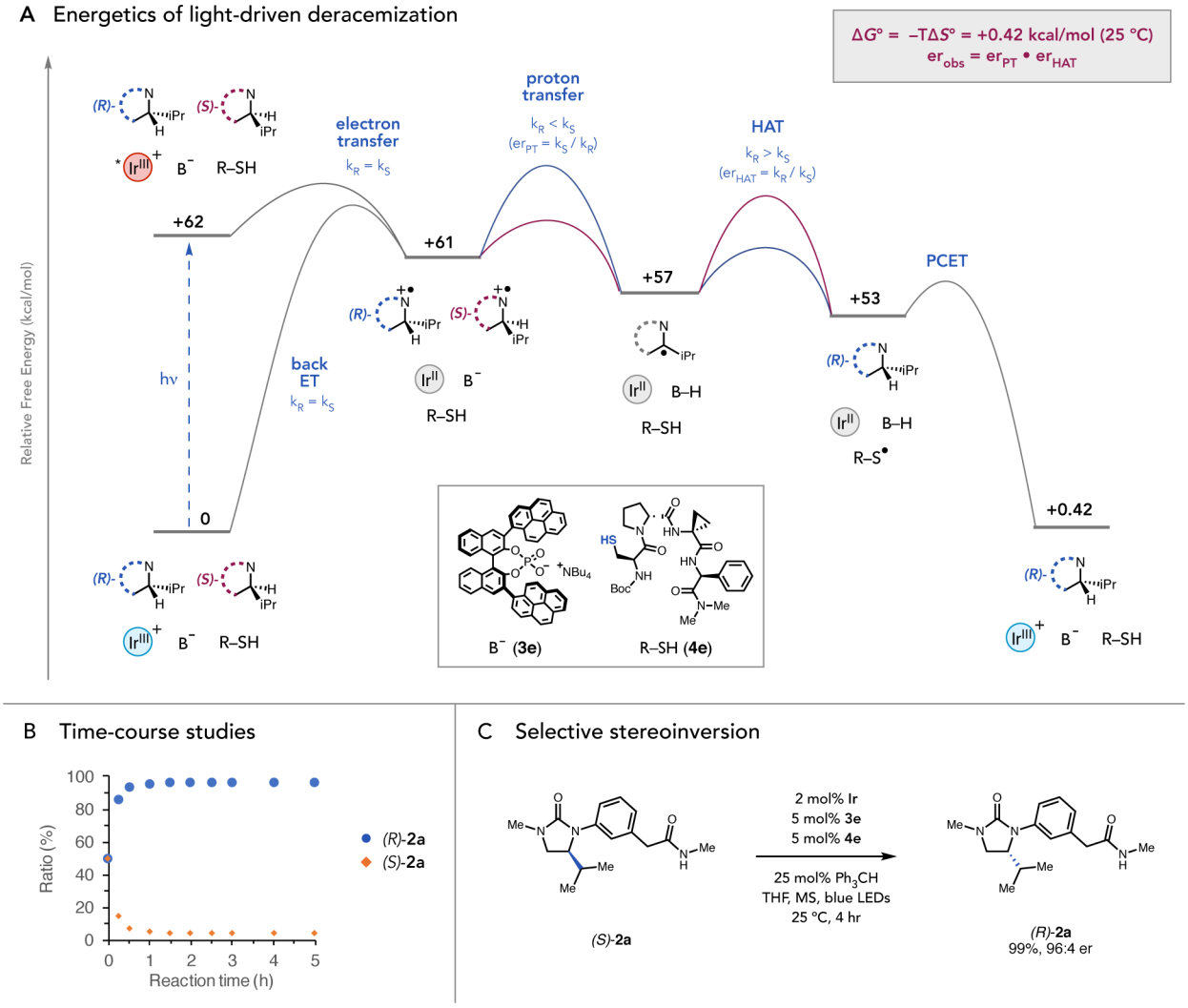

Fig. 4. Preliminary mechanistic studies.

(A) Free energy profile of light-driven deracemization from *rac*-**2a** to (*R*)-**2a**. Details included in supplementary materials. (Fig. S3) (B) Time-course studies for deracemization of *rac*-**2a** to (*R*)-**2a**. (C) Selective stereoinversion of (*S*)-**2a** to (*R*)-**2a**.

Table 1.
Studies on enantioselectivity of each chiral catalyst and synergistic stereoselectivity.

Reaction conditions: 2 mol% Ir, 10 mol% **3e**, 10 mol% PhSH, MS, THF, blue LEDs, 25 °C, 4 h (column 3), 2 mol% **Ir**, 10 mol% $NBu_4^+(PhO)_2P(O)O^-$, 10 mol% **4e** (or *ent*-**4e**), 50 mol% Ph_3CH, MS, THF, blue LEDs, 25 °C, 4 h (column 4), 2 mol% **Ir**, 5 mol% **3e**, 5 mol% 4e (or *ent*-**4e**), 25 mol% Ph_3CH, MS, THF, blue LEDs, 25 °C, 4 h (column 6). The reaction yields in all cases are >90%. Detailed experimental results are included in supplementary materials. (Table S7)

Studies on synergistic enantioselectivity

entry	substrate	exptl. er (er_{PT}) *chiral base only*	exptl. er (er_{HAT}) *chiral thiol only*	predicted er (er_{PT} • er_{HAT})	exptl. er (er_{obs}) *chiral base + chiral thiol*
1	**2a**	86:14	79:21	96:4	96:4
2	**2a**	86:14	21:79 (*ent*-**4e**)	62:38	53:47
3	**2b**	77:23	85:15	95:5	95:5
4	**2d**	80:20	76:24	93:7	92:8
5	**2f**	89:11	69:31	95:5	94:6
6	**2g**	88:12	77:23	96:4	96:4
7	**2h**	87:13	69:31	94:6	93:7
8	**2j**	85:15	81:19	96:4	95:5
9	**2k**	85:15	79:21	96:4	95:5
10	**2m**	83:17	83:17	96:4	95:5
11	**2o**	58:42	79:21	84:16	81:19
12	**1b**	49:51	77:23	76:24	74:26